

AD-A122 421

STABILITY AND SYMMETRY IN INERTIAL CONFINEMENT FUSION  
(U) NAVAL RESEARCH LAB WASHINGTON DC M H EMERY ET AL.  
09 DEC 82 NRL-NR-4947

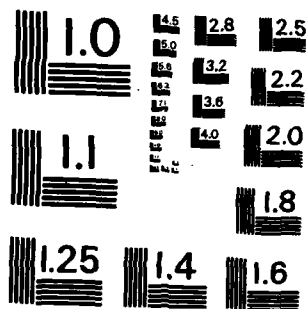
1/1

UNCLASSIFIED

F/G 20/8

NL

END  
DATE  
FILMED  
1 83  
DT 6



MICROCOPY RESOLUTION TEST CHART  
NATIONAL BUREAU OF STANDARDS-1963-A

AD A 122 421

SECURITY CLASSIFICATION OF THIS PAGE (When Data Entered)

REPORT DOCUMENTATION PAGE		READ INSTRUCTIONS BEFORE COMPLETING FORM
1. REPORT NUMBER NRL Memorandum Report 4947	2. GOVT ACCESSION NO. AD-A122 421	3. RECIPIENT'S CATALOG NUMBER
4. TITLE (and Subtitle)  STABILITY AND SYMMETRY IN INERTIAL CONFINEMENT FUSION		5. TYPE OF REPORT & PERIOD COVERED Interim report on a continuing NRL problem.
7. AUTHOR(s) M.H. Emery, S.E. Bodner, J.P. Boris, D.G. Colombant, A.L. Cooper, M.J. Fritts, J.H. Gardner and W.H. Manheimer		6. PERFORMING ORG. REPORT NUMBER
9. PERFORMING ORGANIZATION NAME AND ADDRESS Naval Research Laboratory Washington, DC 20375		8. CONTRACT OR GRANT NUMBER(s)
11. CONTROLLING OFFICE NAME AND ADDRESS Department of Energy      Office of Naval Research Washington, DC 20545      Arlington, VA 22217		10. PROGRAM ELEMENT, PROJECT, TASK AREA & WORK UNIT NUMBERS DEAI088610; 44-1340-0-2; DEAI0879DP; 44-0575-A-2; NR334-002; 44-0573-0-2
14. MONITORING AGENCY NAME & ADDRESS (if different from Controlling Office)		12. REPORT DATE December 9, 1982
		13. NUMBER OF PAGES 17
		15. SECURITY CLASS. (of this report) UNCLASSIFIED
		15a. DECLASSIFICATION/DOWNGRADING SCHEDULE
16. DISTRIBUTION STATEMENT (of this Report)  Approved for public release; distribution unlimited.		
17. DISTRIBUTION STATEMENT (of the abstract entered in Block 20, if different from Report)		
18. SUPPLEMENTARY NOTES This paper was prepared for presentation at the 9th International Conference on Plasma Physics and Controlled Nuclear Fusion Research, Baltimore, MD, USA, 1-8 September 1982. This research was supported by the U.S. Department of Energy and the Office of Naval Research.		
19. KEY WORDS (Continue on reverse side if necessary and identify by block number)  Laser ablation      Inertial confinement fusion Rayleigh-Taylor      Computational fluid dynamics Kelvin-Helmholtz      Hydrodynamic instabilities Wavelength scaling      Inertial fusion targets		
20. ABSTRACT (Continue on reverse side if necessary and identify by block number) The asymmetries of spherical implosions driven by direct laser illuminations are of fundamental concern to the inertial confinement fusion community because they provide severe limitations on high gain pellet designs. Theoretical progress on several fronts has recently been made through numerical simulations in providing a more complete understanding of the physical processes involved in these asymmetries and instabilities. The results also suggest methods of controlling these processes and their implications for laser fusion systems design. Stability and symmetry issues have been investigated.		

(Continues)

DD FORM 1473  
1 JAN 73

EDITION OF 1 NOV 68 IS OBSOLETE  
S/N 0102-014-6601

SECURITY CLASSIFICATION OF THIS PAGE (When Data Entered)

20. ABSTRACT (Continued)

using an adaptively gridded two-dimensional fully nonlinear Eulerian computer model (FAST2D) and a triangular grid Lagrangian computer model (SPLISH). Laser matter coupling and scaling laws relating the asymmetry results to spherical pellet designs have been investigated using a one dimensional sliding zone adaptive gridding fluid code (FAST1D). Principle results include finding (1) the requirements for thermal smoothing of laser nonuniformities, (2) reduced Rayleigh-Taylor growth rates and saturation via the nonlinear Kelvin-Helmholtz roll-up, (3) that perturbation wavelengths greater than the shell thickness are most likely to cause an asymmetric implosion, (4) a new theory based on vortex shedding that explains the reduced linear Rayleigh-Taylor growth rates and (5) a possible wavelength-intensity window for direct illumination where the requirements of pellet velocity, symmetry, and efficiency necessary for high gain can be simultaneously met.

## CONTENTS

I. SYMMETRY .....	1
II. STABILITY - NONLINEAR .....	2
III. STABILITY - LINEAR .....	3
IV. THREE-LAYER RT PROBLEM .....	5
V. WAVELENGTH-INTENSITY WINDOW .....	6
REFERENCES .....	14

Accession For	
NTIS GRA&I	<input checked="checked" type="checkbox"/>
DTIC TAB	<input type="checkbox"/>
Unannounced	<input type="checkbox"/>
Justification	
By _____	
Distribution/	
Availability Codes	
Dist	Avail and/or Special
<b>A</b>	



## STABILITY AND SYMMETRY IN INERTIAL CONFINEMENT FUSION

### I. Symmetry

The critical consideration for achieving high spherical compression is to determine the symmetry requirements on the driver imposed by the symmetry that can be maintained during the implosion process. Ablation pressure symmetry with  $\Delta p/p < \text{few percent}$  must be maintained if high gain is to be achieved<sup>1</sup>. We have investigated the effect of an asymmetric laser beam ( $1.05 \mu\text{m}$ ) with an intensity ratio  $I_{\text{max}}/I_{\text{min}} \approx 2$  on thin foils ( $15 \mu\text{m CH}$ ) with our FAST2D code<sup>2</sup>. We find that lateral energy flow in the form of transverse thermal conduction smooths the effects of laser asymmetries. The degree of smoothing is directly related to the distance between the ablation and critical surfaces. To smooth asymmetries to the extent that the ablation pressure variation is less than a few percent requires that the scale length of the asymmetry be comparable to the distance between the ablation and critical surface.

The numerical results are summarized in Fig. 1., where the variation in ablation pressure is plotted as a function of the average laser intensities for a series of asymmetry scalelengths ( $\lambda_L$ ) in the range of  $100 \mu\text{m} < \lambda_L < 600 \mu\text{m}$ . (Also shown is the equivalent distance between the ablation surface and the critical surface.) These results are in agreement with the NRL experimental results<sup>3</sup> shown in Fig. 2. We compare the foil velocity nonuniformity ( $v_{\text{max}}/v_{\text{min}} - 1$ ) for the 100 and 200  $\mu\text{m}$  asymmetries to the experimental results for a 140  $\mu\text{m}$  asymmetry with  $I_{\text{max}}/I_{\text{min}} \approx 2$ .

A new analytic steady-state planar ablative flow model<sup>4</sup> has been developed from which scaling laws can be derived which depend only on the material, laser wavelength and absorbed laser irradiance. The derived scaling

Manuscript approved September 20, 1982.

laws are in good agreement with both experiment and fluid simulations. On Fig. 2 we show the results of the analytic model for laser smoothing.

## II. Stability - Nonlinear

The Rayleigh-Taylor(RT) instability may also destroy the spherical symmetry of high aspect ratio imploding shells. This desymmetrizing instability may grow in the ablation layer or at an internal interface where materials of different densities abut. Using our FAST2D code we have modelled the RT instability far into the nonlinear regime and beyond the point of foil fragmentation for both a multimode perturbation<sup>5</sup> and for single mode perturbations for a series of perturbation wavelengths ( $\lambda$ ) in the range of  $1/2 < \lambda/AR < 10$ , where  $AR$  is the cold foil thickness (20  $\mu m$ ). Laser intensities were in the range  $1-5 \times 10^{13}$  W/cm<sup>2</sup>.

We find linear growth rates well below classical values (by a factor on the order of 3-4) and a cutoff in the growth rate for wavelengths less than the cold foil thickness. The striking result is the dominance of nonlinear effects, i.e., the Kelvin-Helmholtz (KH) roll-up, for short wavelength perturbations. Although the linear growth rates increase as  $k^{1/2}$  up to the cutoff, the KH roll-up dominates at large  $k$ , drastically reducing the penetration rate of the dense spike below its free fall value and effectively doubling the aspect ratio of the foil<sup>6</sup>.

The growth rate of the spike shifts from exponential to quadratic (free-fall) when the amplitude of the disturbance is on the order of  $1/5$  the wavelength [ $A \sim 0(0.2 \lambda)$ ]. As a result, the amplitude of the large wavelength modes ( $\lambda/AR > 1.25$ ) goes into "free-fall" at a later time and with an effective "free-fall" acceleration comparable to the foil acceleration [ $0(1.5 \times 10^{15}$  cm/s<sup>2</sup>)]. The exponential growth of the short wavelength modes

( $\lambda/AR \leq 1.25$ ) saturates earlier in time (since the linear growth rate is larger) and the "free-fall" acceleration of the spike is reduced. This reduction is a direct consequence of the tip-widening brought on by the KH roll-up. The frontal area of the spike is increased thereby increasing its drag and reducing its rate of fall.

These results have serious implications with respect to shell integrity as a function of perturbation wavelength. This is evident from Fig. 3 where both the "free-fall" acceleration of the spike and the final aspect ratio of the foil are plotted as a function of perturbation wavelength ( $\lambda/AR$ ). Note that the "free-fall" acceleration ("g") of the spike is reduced by over a factor of two for the short wavelengths. A combination of the reduced "free-fall" and the earlier exponential growth saturation increases the aspect ratio ( $R/AR$ ) of the short wavelength perturbation by a factor of two over the long wavelength modes. Thus nonlinear effects, in the form of the KH roll-up, dominate at large  $k$ , saturating the linear  $k^{1/2}$  form of the RT instability, reducing the rate of "fall" of the spike and increasing the aspect ratio of the foil before breakup.

### III. Stability - Linear

We now show that the vorticity, which plays such a dominant role in the nonlinear evolution of the RT instability, is also responsible for the reduced linear growth rates. In particular, it is the shedding of the vorticity generated at the ablation layer that gives rise to the low values of the growth rate<sup>7</sup>.

Figure 4 shows the vortex shedding process from the ablation layer for the 20  $\mu$ m perturbation wavelength when the system is in the linear regime. The finite-sized vortices are generated by the baroclinic (non-collinear

density and pressure gradients) nature of the profiles. The vorticity generated at the ablation surface is then convected with the flow and shed into the blowoff. This shedding process is very similar to the shedding of the vortex structure that arises from the flow about a bluff body and the measured Strouhal number (dimensionless shedding frequency) agrees very well with this theory. The shedding process reduces the classical RT growth rate by removing some of the vortex motion from the growth region. We express this reduced growth rate as  $\gamma' = (kg)^{1/2} - \alpha f$ , where  $f$  is the measured shedding frequency and  $\alpha$  is some fraction (less than one). Figure 5 compares this result with the computational growth rates.

Not only does this shedding reduce the linear RT growth rate but a symmetric von Karman vortex street develops in the blow off region. The symmetric vortex street is very unstable and this structure could have serious effects on laser absorption, thermal conduction and plasma instabilities in the underdense region.

Vorticity continues to be shed from the ablation layer until the spike amplitude becomes comparable to half the perturbation wavelength and the bubble region ceases to ablate. The vorticity is then advected down the sides of the spikes where it sets up a reversed flow which causes the tips of the spike to widen thus reducing their penetration rate. Vortex dynamics plays a dominant role in both the linear and nonlinear phases of the RT instability.

We have also simulated the linear and nonlinear evolution of the RT instability for strongly perturbed targets and these results are presented elsewhere at this conference<sup>8</sup>.

#### IV. Three-Layer RT Problem

The interior-layer Rayleigh-Taylor problem can occur at many different times and locations during the implosion of a complicated multiple-shell target. The preignition mix problem is the most familiar situation. This occurs near the final stages of compression of the fuel when the interface between the higher density pusher and the fuel compressionally decelerates. A three-layer mix problem arises where a light fuel layer is separated from a denser pusher shell by a thin but very dense heat-shield layer. Short-wave-length perturbations permit the upper and lower surfaces of the heat shield to move independently, so the RT instability can result even though overall stability is expected at long wavelengths. In order to investigate the non-linear regime of the RT instability for these two- and three-layer mix problems we have developed a Lagrangian model (SPLISH) which bases its fluid representation on a two-dimensional dynamically reconnectable grid of triangles<sup>9</sup>.

In the three layer mix problem the densities of the layers are in the ratio 0.1:2:1 so that the unstable interface has an Atwood number of 1/3. At this Atwood number the evolution of the unstable interface is governed by the interaction between the RT and KH instabilities in both the linear and non-linear regimes. The evolution of the RT and KH instabilities can be separated into four distinct phases: (1) the initial classical, linear growth phase, ending when the spike to bubble height is half the perturbation wavelength, or for thin layers, when the spike to bubble height equals the layer thickness; (2) a saturated RT growth phase with steadily increasing KH roll-up and increasing wavelength, ending when the spike tip becomes wider than the spike body; (3) a small scale structure phase and (4) a turbulent mixing

phase. The third phase is characterized by downward flow from the thinned layers above the bubbles resembling jets feeding the spike. A stagnation point forms at the point where the jets collide, forcing an upward jet opposed to the spike fall. In the last phase, large amplitude waves run across the stable interface as well, giving rise to jetting and wave-breaking. Many similarities exist between the ablative and nonablative cases. The KH instability plays a very major role in both cases in that it reduces the penetration rate of the dense spike below its free-fall value.

#### V. Wavelength-Intensity Window

The stability and symmetry results provide limitations on the designs of the laser fusion pellets if high gain is to be achieved. RT results indicate a limit in the aspect ratio of around 40. Symmetry results indicate that the separation distance of the critical from the ablation surface should be about .3 to .5 of the current pellet radius. We have used our one-dimensional code (FAST1D) to investigate scaling laws and find an intensity wavelength window based on these limits <sup>10</sup>.

Calculations at laser wavelengths of 0.53, 1.06, and 2.7  $\mu\text{m}$  with pellet radii of 1, 2, and 5 mm were used to derive scaling laws for the pressure  $P$  and the separation ratio  $D/R$  versus laser intensity, laser wavelength, and pellet radius. We find a pressure scaling of the form  $P \sim (I_a^{-0.25} R^{-0.18})^{0.7}$ , and a separation ratio scaling of the form  $D/R \sim (I_a \lambda^{3.8})^{0.7} / (R+B)$ . In the region of interest,  $B \approx 1$  mm, and is only weakly dependent on  $I_a$  and  $\lambda$ . This form goes to the correct limits for both large and small radii.

Our symmetry results indicate that if the separation distance  $D$  is more than 2.3 times the laser inhomogeneity wavelength, then  $\delta P/P < .16 I/I$  ( $P = 1$ ), providing sufficient for 10% laser nonuniformities.

For today's moderate aspect-ratio pellet, with  $R_0/\Delta R_0 = 8-20$ , an ablation pressure of about 10-30 Mbar is required to drive the shell inward to fusion-level velocities, with use of a relatively unshaped laser pulse. Figure 6 shows the minimum smoothing and pressure barriers based on these limits. The optimal laser intensity is approximately a few times  $10^{14}$  W/cm<sup>2</sup> and at approximately one-micron laser wavelength. This should suffice for producing both sufficient ablation pressure and sufficient two-dimensional smoothing. (For a flux limit of  $f = 0.03$  the optimal wavelength would increase to 2-3  $\mu$ m.)

For fixed smoothing decreasing the laser wavelength  $\lambda$  increases the instability parameter  $I\lambda^2$  increasing the potential for plasma instabilities. Equally important, the high ablation pressure at large intensities might be too large thereby driving strong shocks that would preheat the pellet.

There seems to be a barrier at shorter wavelengths because the smoothing requirement quickly drives one to unacceptably high laser intensities and ablation pressures. And at longer wavelengths, the ablation pressure requirement on the laser intensity soon exceeds the threshold for plasma instabilities. The actual location of the wavelength window is somewhat uncertain, but it appears to lie between 1/2 and 2.7  $\mu$ m.

Another important consideration in parameter mapping is the hydrodynamic efficiency. In Fig. 6 we also show the variation of intensity with laser wavelength for fixed hydrodynamic efficiency. Efficiencies greater than 7% are achieved below this line. The highest efficiency is achieved by operating at the intersection of the smoothing requirement and the pressure limitations.

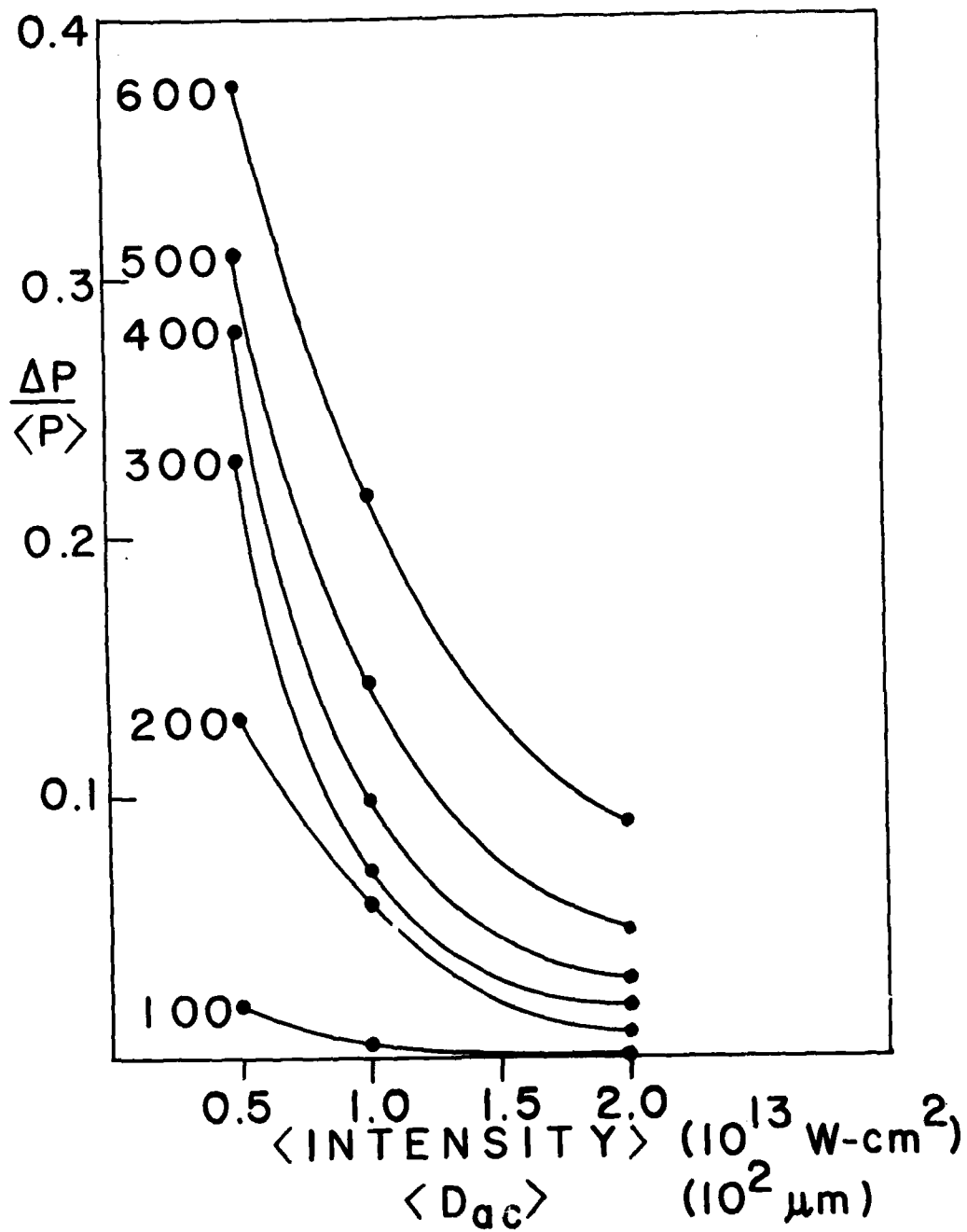


Fig. 1 — The variation in ablation pressure ( $\Delta p/p$ ) for all six scale lengths plotted as a function of the average laser intensity ( $\langle I \rangle$ ) and as a function of the average distance from the ablation surface to the critical surface ( $\langle D_{ac} \rangle$ ).

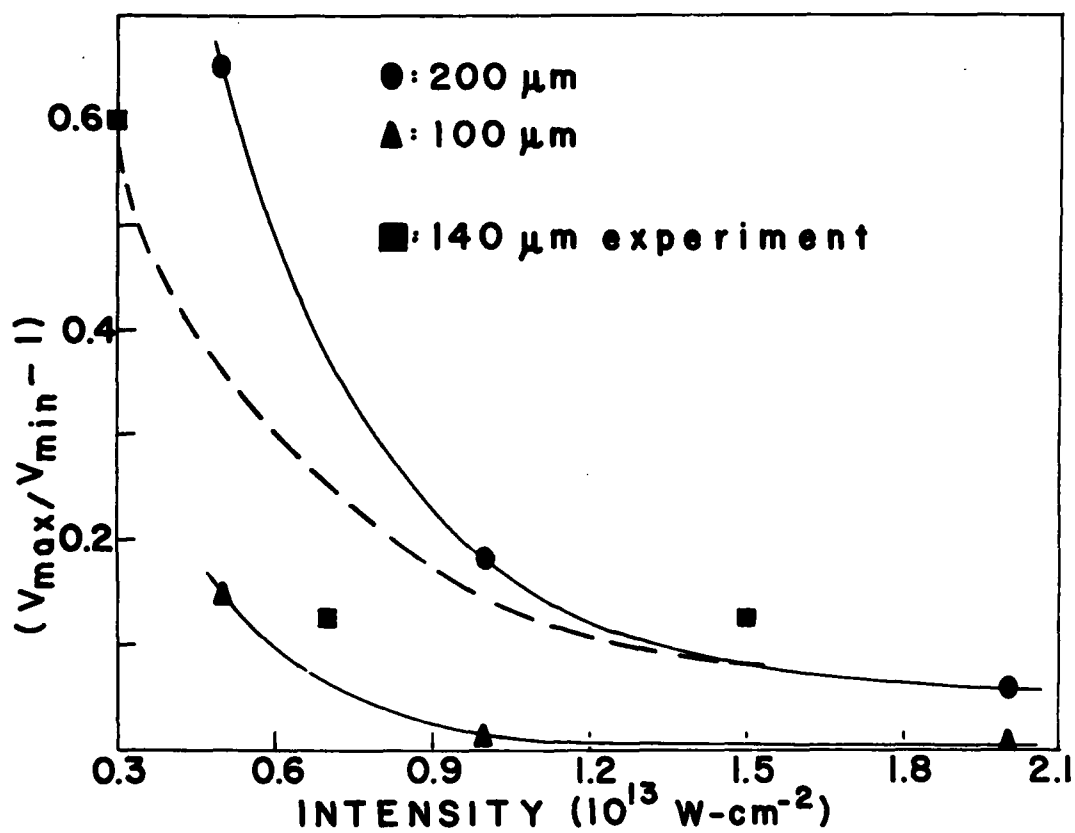


Fig. 2 — Comparison of the numerical results for the 100- and 200  $\mu\text{m}$  scale lengths with the 140  $\mu\text{m}$  scale length experimental results (Ref. 3) and with the 140  $\mu\text{m}$  theoretical results (dashed curve, Ref. 4).

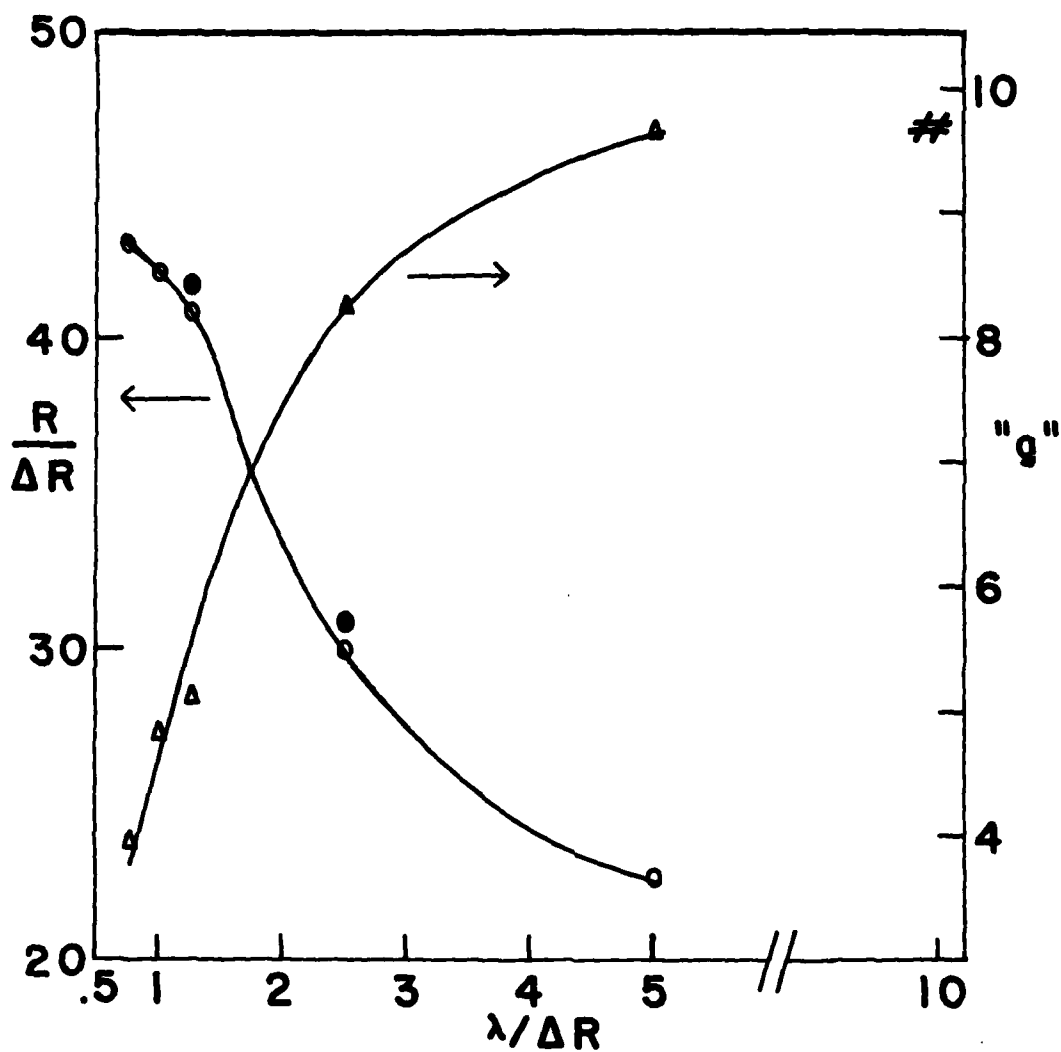


Fig. 3 — A plot of the "free-fall" acceleration ("g" in units of  $10^{14}$  cm/s<sup>2</sup>) of the spike and the final aspect ratio of the foil as a function of the perturbation wavelength ( $\lambda/\Delta R$ ). The solid circles are the aspect ratios obtained with a laser intensity of  $5 \times 10^{13}$  W/cm<sup>2</sup> and the # symbol is the aspect ratio obtained with a perturbation wavelength of 200  $\mu$ m.

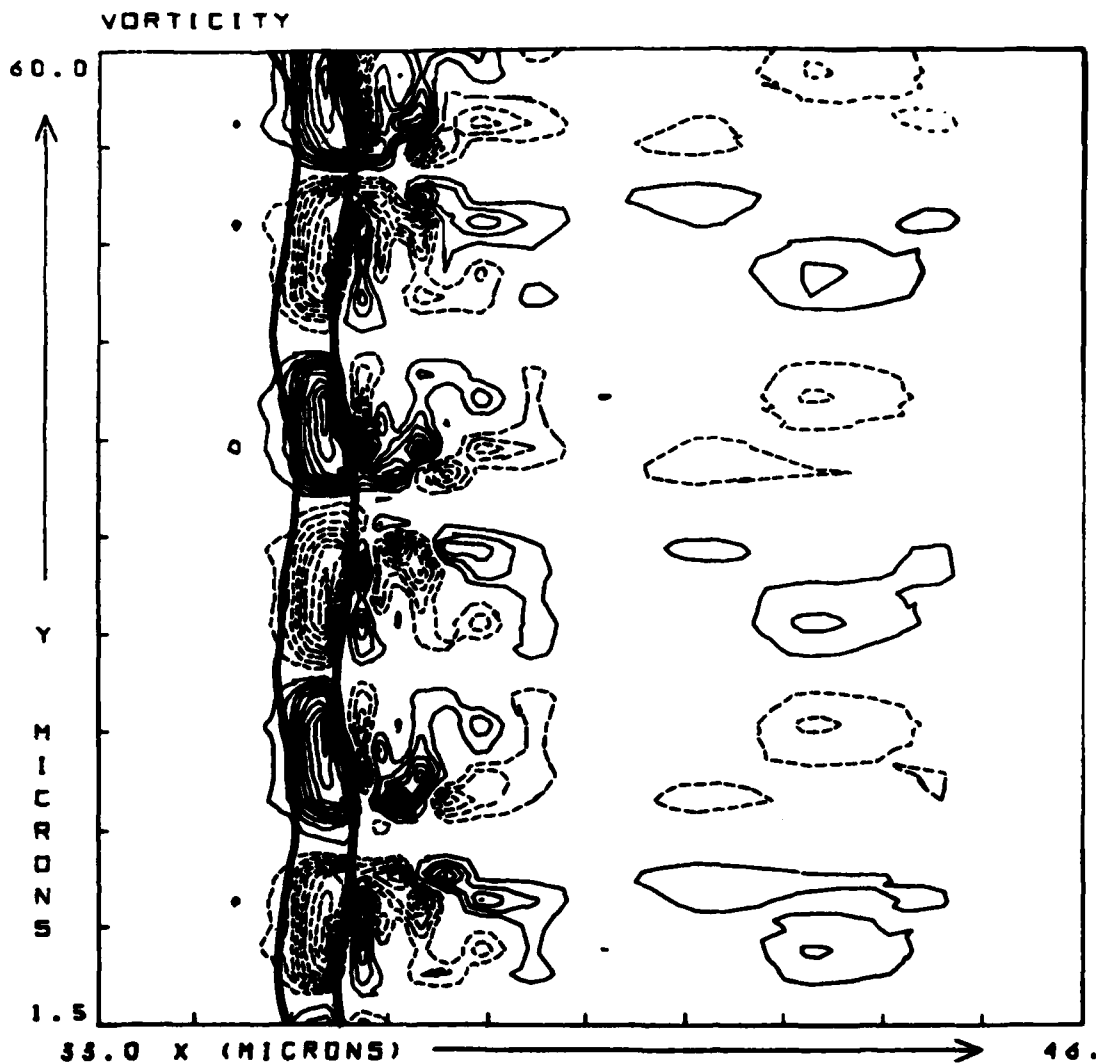


Fig. 4 — Vorticity contours for the 20  $\mu\text{m}$  mode ( $\lambda/\Delta R = 1$ ) when the system is in the linear regime. The contours are in 10% increments of the maximum vorticity ( $+2.75 \times 10^8$ ,  $-2.87 \times 10^8 \text{ S}^{-1}$ ). The solid (dashed) contours are positive (negative) vorticity. The heavy lines delineate the 10% (right) and 90% (left) density contour.

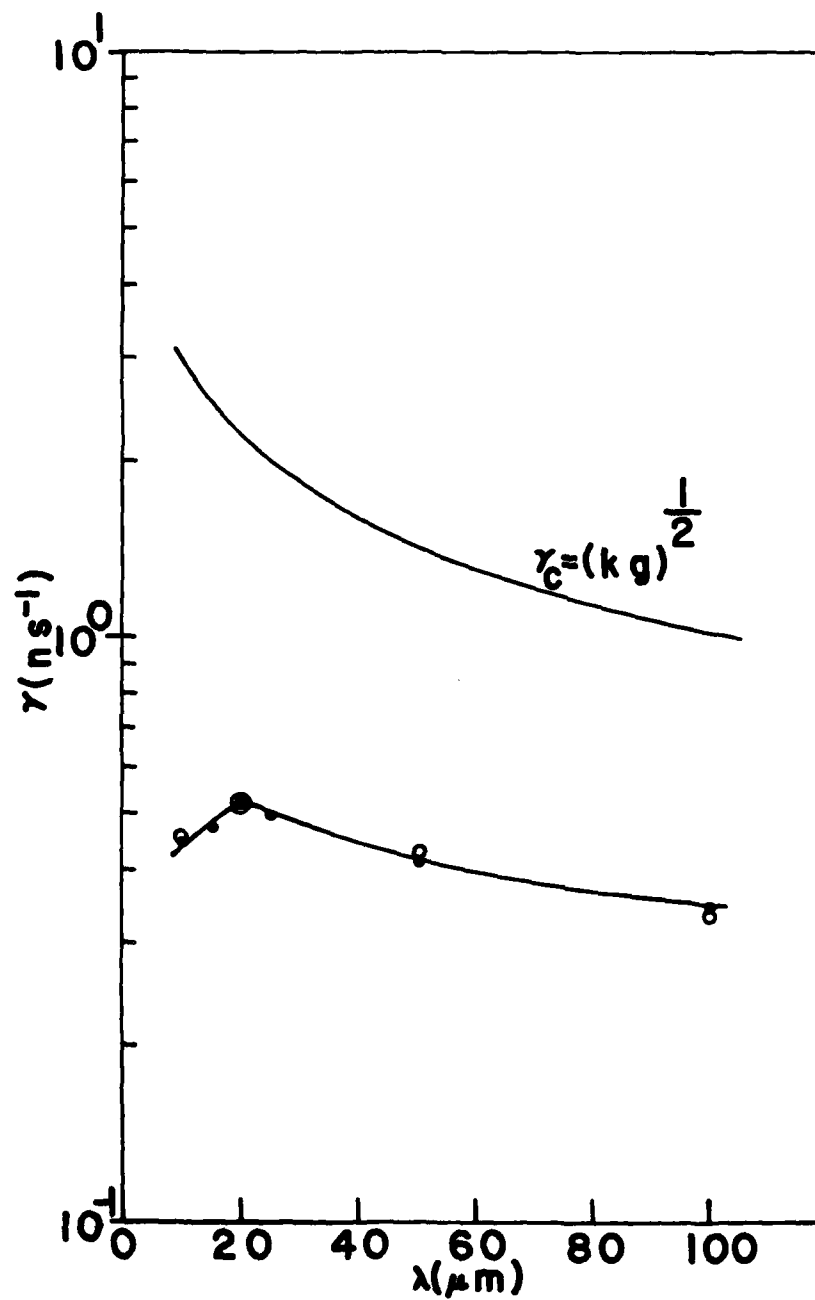


Fig. 5 — A comparison of the computational growth rates ( $\bullet$ ) to the classical value  $((kg)^{1/2}, \text{—})$  and to the vortex shedding theory ( $\circ$ ). ( $\alpha = 0.56$  to fit the  $20 \mu\text{m}$  mode).

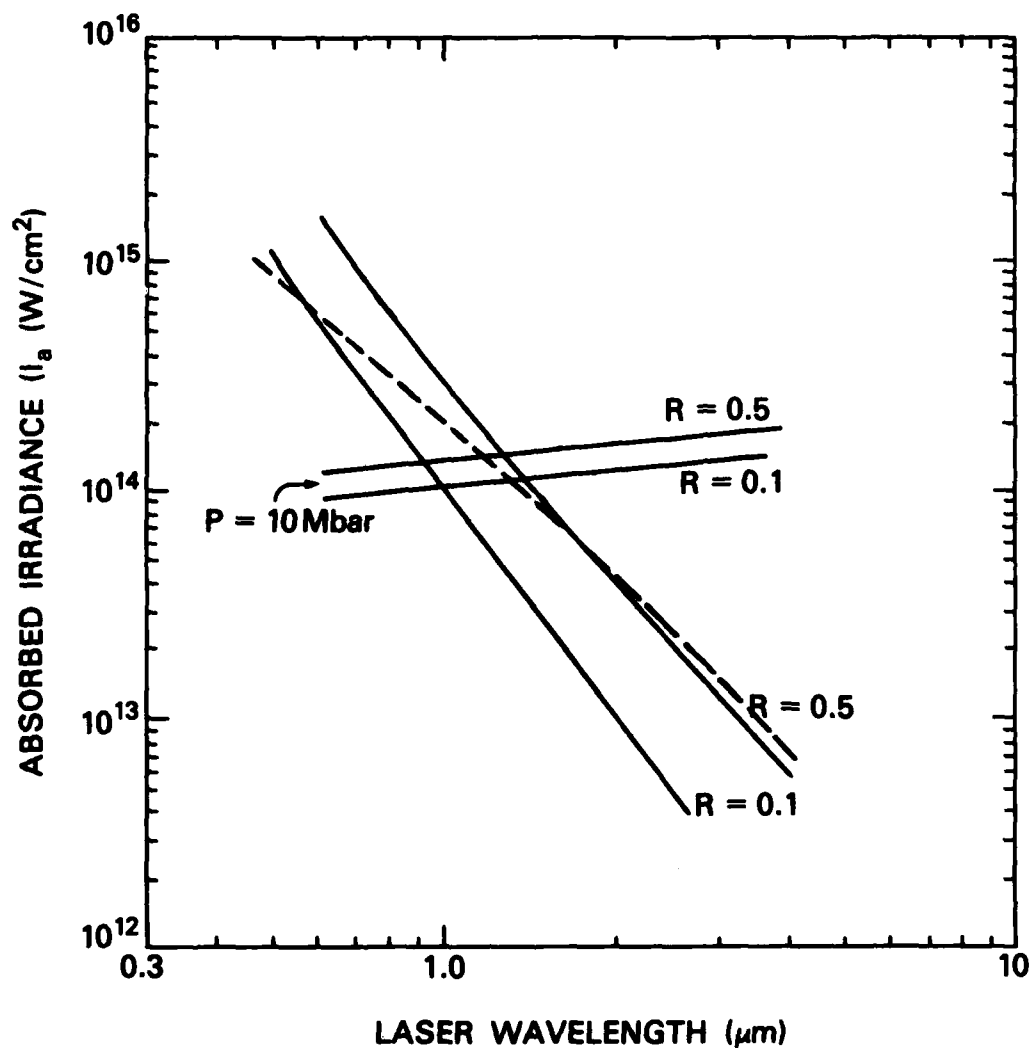


Fig. 6 — Wavelength-intensity window determined by the symmetry requirements (downward sloping solid curves) and the stability limits (aspect ratio  $< 40$ ) for two radii pellets (.1 and .5 cm). Constant efficiency of 7% is shown by dashed line. Operating region is the upper right hand quadrant.

## REFERENCES

- [1] J. Nuckolls et al., *Nature* (London) 239 (1972) 139.
- [2] M.H. Emery et al., *Phys. Rev. Lett.* 48 4 (1982) 253.
- [3] S.P. Obenschain et al., *Phys. Rev. Lett.* 46 (1981) 1402.
- [4] W.M. Manheimer et al., Naval Research Laboratory Memorandum Report No. 4644 (1981). (Submitted to *Phys. Fluids*).
- [5] M.H. Emery et al., *Phys. Rev. Lett.* 48 10 (1982) 677.
- [6] M.H. Emery et al., Naval Research Laboratory Memorandum Report No. 4882 (1982). (Submitted to *App. Phys. Lett.*)
- [7] M.H. Emery et al., 12th Annual Anomalous Absorption Conf., Santa Fe (May, 1982).
- [8] B.H. Ripin et al., "Laser-Ablative Acceleration of Targets to Near Fusion Conditions" (Proc. 9th Int. Conf. on Plasma Phys. and Cont. Nuc. Fus. Res., 1982), IAEA, Baltimore (1982).
- [9] M.J. Fritts and J.P. Boris, *J. Comp. Phys.* 31 (1979) 173.
- [10] J.H. Gardner and S.E. Bodner, *Phys. Rev. Lett.* 47 16 (1981) 1137.

DATE  
TIME